JOURNAL OF MATERIALS SCIENCE 24 (1989) 1782–1794

Solute redistribution in stir-cast Al–6Cu

J. M. M. MOLENAAR, W. H. KOOL
Laboratory of Metallurgy, Delft University of Technology, Rotterdamseweg 137, 2628 AL Delft, The Netherlands

The solute distribution in stir-cast Al–6 wt% Cu alloy is more uniform than that in the conventionally cast (unstirred) alloy, solidified at the same cooling rate. The Bower–Brody–Flemings model of microsegregation was modified to take account of convective interdendritic (or intercellular) solute transport in the liquid. It was found that the modified model allows a reasonable description of the observed solute distribution in both the stirred and the unstirred alloy. Differences are described in terms of two parameters: the dendrite tip undercooling constant a and the effective equipartition ratio k_e, which includes the influence of convective solute transport. It is concluded that the solute distribution is more uniform the greater either of these constants becomes.

1. Introduction

It has been established [1–7] that when alloys are stirred during solidification, the solid which forms has a special non-dendritic structure. In contrast, unstirred alloys normally solidify dendritically. Previous papers [8–10] have dealt with an investigation of the growth morphology of stir-cast Al–6 wt % Cu. This paper is concerned with measurements of the solute distribution in the primary solid phase formed in the first stage of the solidification of Al–6Cu during stir-casting (i.e. prior to quenching). The aim is to analyse and describe the difference in microsegregation in stirred and unstirred Al–6Cu. In particular, attention is given to the influence of convection on the redistribution of solute in the solid phase, during solidification. The Bower–Brody–Flemings (BBF) model of microsegregation was modified to take account of convective solute transport in the liquid. In the original version [11], only diffusion in the liquid was considered, while diffusion in the solid was neglected. The experimental results are compared with the predictions of a diffusion model in which the modified BBF model, the Scheil model [12], or the Brody–Flemings (BF) model [13] are used as boundary conditions for the solute concentration in the solid at the interface. The Scheil model assumes no diffusion in the solid and complete diffusion in the liquid. The BF model as modified by Clyne and Kurz [14] describes the back-diffusion in the solid when diffusion in the liquid is complete. The BBF model assumes no diffusion in the solid and limited diffusion in the liquid. The modified BBF model includes the effect of a constant convective flow of solute in the intercellular liquid.

2. Experimental details

The specimens investigated in this work were obtained from stir-casting experiments described previously [8]. Here, only a brief review of these experiments is given. A series of batch-type stirring experiments was performed in which Al–6Cu alloy was continuously cooled and solidified in an annular space between two concentric cylinders, the inner of which was rotating. Different cooling rates and stirring speeds were applied. In all experiments stirring was stopped and the sample was quenched when the volume fraction of solid was about 50%. The total solidification time is defined as the time spent between the recorded nucleation event and the moment when the temperature fell below the eutectic temperature. The total solidification time varied between 8 and 2700 sec. In all stirred samples the typical non-dendritic stir-cast structure was found. At long stirring times, the primary particles consist of agglomerated cells. At short stirring times also, typical rosette-type particles are observed.

Two reference experiments were performed without stirring; one with a total solidification time of 8 sec (water-quenched), the other with a total solidification time of 380 sec (naturally cooled).

Both stirred and unstirred specimens were subjected to electron microprobe analysis, applying a Jeol JXA 50A instrument. Copper concentrations were determined from point analysis measurements applying ZAF correction procedures. Also continuous line-scans were taken. The traces along which the Cu$K\alpha$ intensity was measured were chosen preferably in two perpendicular directions, as indicated schematically in Fig. 1. Fig. 1c shows a dendrite which is typical for the conventional (unstirred) structure. Fig. 1a shows a typical rosette structure observed in stir-cast specimens, and Fig. 1b shows an "agglomerated particle", also typical of the stir-cast structure. In each case, Trace L is in longitudinal direction, i.e. along secondary dendrite arms, along cellular arms, or along cells in radial direction in agglomerated particles. Similarly, Trace T is in the transverse direction, i.e. across secondary dendrite arms, cellular arms and radial cells, respectively.

0022–2461/89 $03.00 + .12

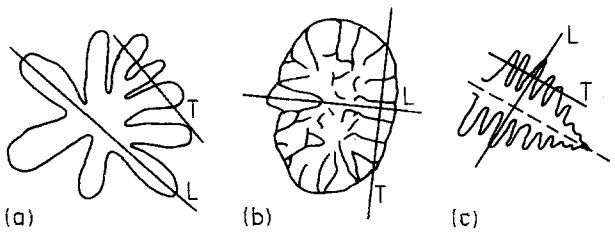

Figure 1 Schematic diagram of morphology of primary particles and types of trace for X-ray microanalysis: (a) rosette, (b) particle consisting of agglomerated cells, (c) dendrite. L and T mark traces in the longitudinal and transverse direction, respectively.

3. Experimental results

3.1. Solute distribution in stir-cast Al–6Cu

In this section, some representative examples of solute distribution profiles are described, selected from stirred specimens. Thee are two typical particle morphologies observed: the rosette-type and the "agglomerated particle" type. Solute concentrations were measured along traces in longitudinal and transverse directions. In total, 24 profiles from 11 stirred specimens were obtained. The minimum solute concentration observed in these profiles are summarized in Table I, together with the solidification times of the samples. From this table the following observations can be made: (i) the minimum solute level is not significantly different in the longitudinal and transverse directions, and (ii) the minimum solute level is independent of the solidification time. The average minimum solute concentration for all segments was found to be 1.4 wt %. The observed microstructures show the typical characteristics of the cellular structure described by Sharp and Hellawell [15]. These characteristics are (i) the typical morphology, (ii) the uniformity of the copper concentration in the primary solidified phase, and (iii) the ripening of cells (i.e. the contraction of intercellular liquid and the resulting breakdown of intercellular films).

3.1.1. Quickly cooled samples

Quickly cooled samples are those for which the total solidification time was shorter than 10 sec. The average depression of the initial growth temperature of the solid observed was 14 K. Fig. 2 shows some examples. Fig. 2a shows a trace in the longitudinal direction along two cellular arms of a rosette-type particle. Rosettes are typically observed in specimens obtained at high and intermediate cooling rates [8]. The measured concentration profile is given in Fig. 3a. We observe that the solute concentration is rather uniform over the complete length of the cellular arms. Fig. 2b shows a path in the transverse direction across three cellular arms of a rosette. Along this path the profiles shown in Fig. 3b was obtained. Fig. 3 illustrates that the copper concentration in rosettes is fairly uniform, except near the phase boundaries.

The minimum solute concentrations observed (see Table I) are significantly higher than the value of k_0C_0 ($k_0 = 0.165$) expected in the case of negligible dendrite tip undercooling and solid back-diffusion. A similar observation was made by Doherty *et al.* [16, 17]. They have shown that the initial solute content of the solid formed during solidification depends on the growth temperature, and can be greater than k_0C_0. They observed that the depression of the initial growth temperature is dependent on the heat extraction rate. They also observed the thermal arrest period after nucleation to depend on the tips of dendrites being able to penetrate liquid in an unconstrained manner. In the present study, the initial growth temperatures observed with the quickly cooled samples suggest that the growth temperature of rosettes is depressed, while the initial solute content of the solid is increased accordingly. The observed uniformity of solute distribution in rosettes can be explained by the fact that the growth temperature of the solid is approximately constant during the arrest period just after nucleation [16].

TABLE I Observed minima in solute distribution profiles obtained from stirred and unstirred samples

Type*	Solidification time (sec)	Observed minima† (wt % Cu)				
L	8	1.3 (1)	1.4 (1)	1.7 (2)		
T	8	1.4 (3)	1.5 (1)	1.6 (4)		
R–T	8	1.4 (1)	1.5 (4)	1.7 (4)		
		1.8 (1)	1.9 (1)	2.1 (2)	2.3 (1)	2.6 (1)
T	228	1.3 (2)	1.4 (5)	1.5 (2)	1.7 (2)	
L	228	1.3 (6)	1.4 (8)	1.5 (2)	1.6 (1)	
L	252	1.2 (2)	1.3 (1)			
T	360	1.3 (1)				
L	360	1.2 (1)	1.3 (1)	1.4 (2)	1.6 (1)	
R–T	380	1.6 (3)	1.8 (2)			
L	420	1.3 (3)	1.4 (1)	1.5 (2)	1.6 (1)	1.7 (2)
T	720	1.4 (3)				
L	720	1.4 (2)				
T	780	1.4 (2)				
L	780	1.4 (2)	1.5 (1)			
T	1860	1.6 (1)				
L	1860	1.6 (1)	2.2 (1)			
T	2010	1.3 (1)	1.4 (1)	1.5 (1)		
L	2010	1.3 (1)				

*L = profile(s) is longitudinal direction; T = profile(s) in transverse direction; R = unstirred reference sample.
†A number between brackets indicates the number of times a minimum solute concentration was observed.

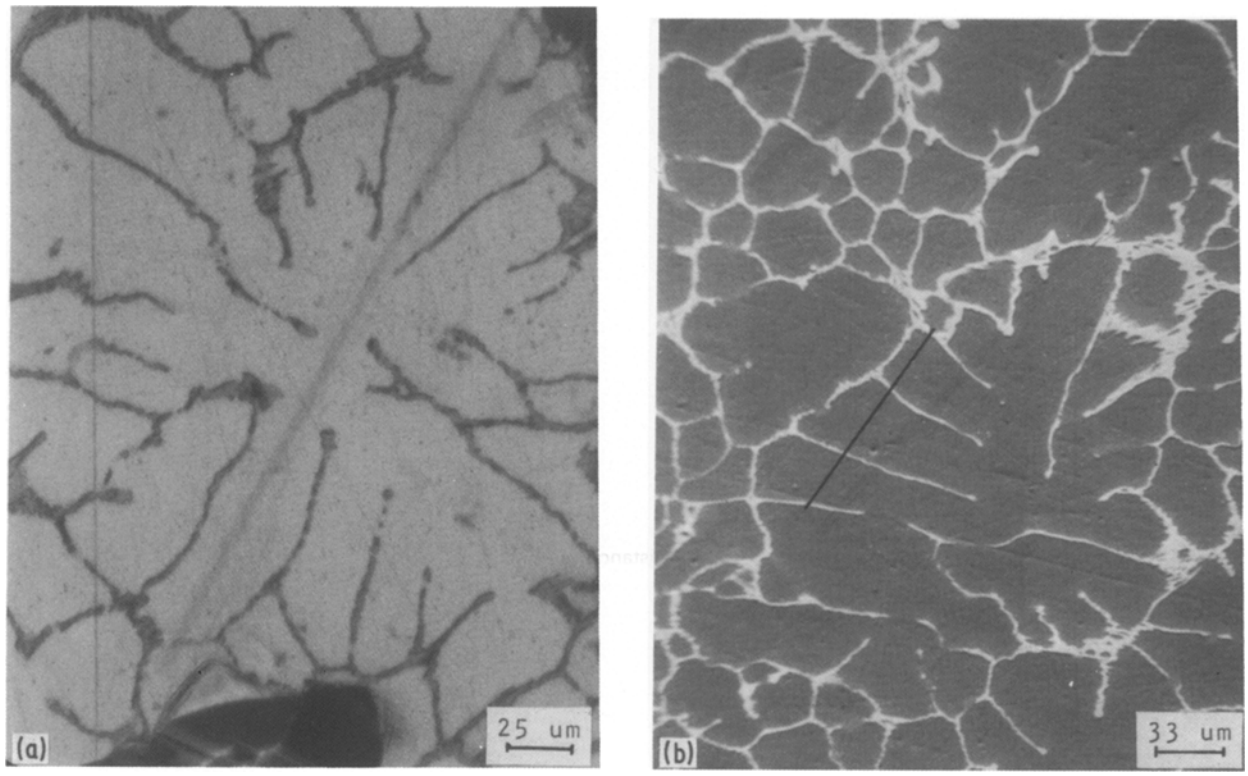

Figure 2 Traces of measurement of Cu$K\alpha$ intensity in quickly cooled stir-cast specimens of Al–6Cu (solidification time 8 sec): (a) longitudinal direction in a rosette, (b) transverse direction in a rosette.

3.1.2. Slowly cooled samples

Slowly cooled samples are those for which the total solidification time was longer than 60 sec. For these samples nucleation undercooling was absent. Fig. 4 shows an example where continuous line-scans were made along two mutually perpendicular traces. Fig. 4a shows a large particle consisting of agglomerated cells of arbitrary shape and presumably – if agglomerated from fragmented parts – arbitrary orientation. Fig. 4b shows the same particle at greater magnification Figs 5a and b show the corresponding profiles. The uniformity of the solute distribution in these examples is characteristic of the stir-cast structure. It can be seen in Fig. 5 that the copper concentration is uniform across the different cells, irrespective of their size, orientation, or the distance between the trace of measurement and nearby phase boundaries. Only in the immediate vicinity of a phase boundary is the copper concentration observed to increase significantly. In addition, the average minimum solute concentrations in the solid correspond to the solidus concentrations given by the phase diagram at the quench temperatures. Based on these observations, it is concluded that the solid and liquid phases are practically in equilibrium during stir-casting at low cooling rate.

3.2. Solute distribution in unstirred Al–6Cu

As already mentioned in Section 2, two reference experiments were performed without stirring. The quickly cooled sample was obtained under the same thermal conditions as the quickly cooled stir-cast samples. The observed depression of the initial growth temperature was 13 K. For the slowly cooled samples, nucleation undercooling was absent.

Figs 6a and b show the microstructures of a quickly cooled and slowly cooled sample, respectively. Figs. 7a and b show profiles obtained from these samples. The minimum solute concentrations in the centres of the secondary dendrite arms are similar to those observed in stirred samples, and are given in Table I. Apart from the solute minima the solute distribution profiles in unstirred samples are clearly different from those observed in stirred samples: (i) the dendrite arm spacing in unstirred samples is typically smaller than the cellular arm spacing in stirred samples, and (ii) the profiles obtained from stirred samples are more uniform. The fact that the cellular arm spacing in the stir-cast alloy is greater than the dendrite arm spacing in the unstirred alloy was shown more generally in previous work [8]. In the following sections the difference between the solute distribution profiles from stirred and unstirred samples will be analysed.

4. Comparison of experimental and calculated results

The aim of this work is to explain the difference in microsegregation in the stirred and unstirred alloys. For this purpose, the solute distribution during solid growth was calculated by solving the diffusion equation for the solute concentration in the solid, in a cylindrical geometry, and using different boundary conditions. For the boundary conditions, the Scheil equation [12], the BF model [13] and the BBF model [11] were applied. Details of the calculations are given in Appendices A and B. The most important assumptions are the following. The Scheil model assumes no diffusion in the solid, and complete diffusion in the liquid. Complete diffusion in the liquid is often

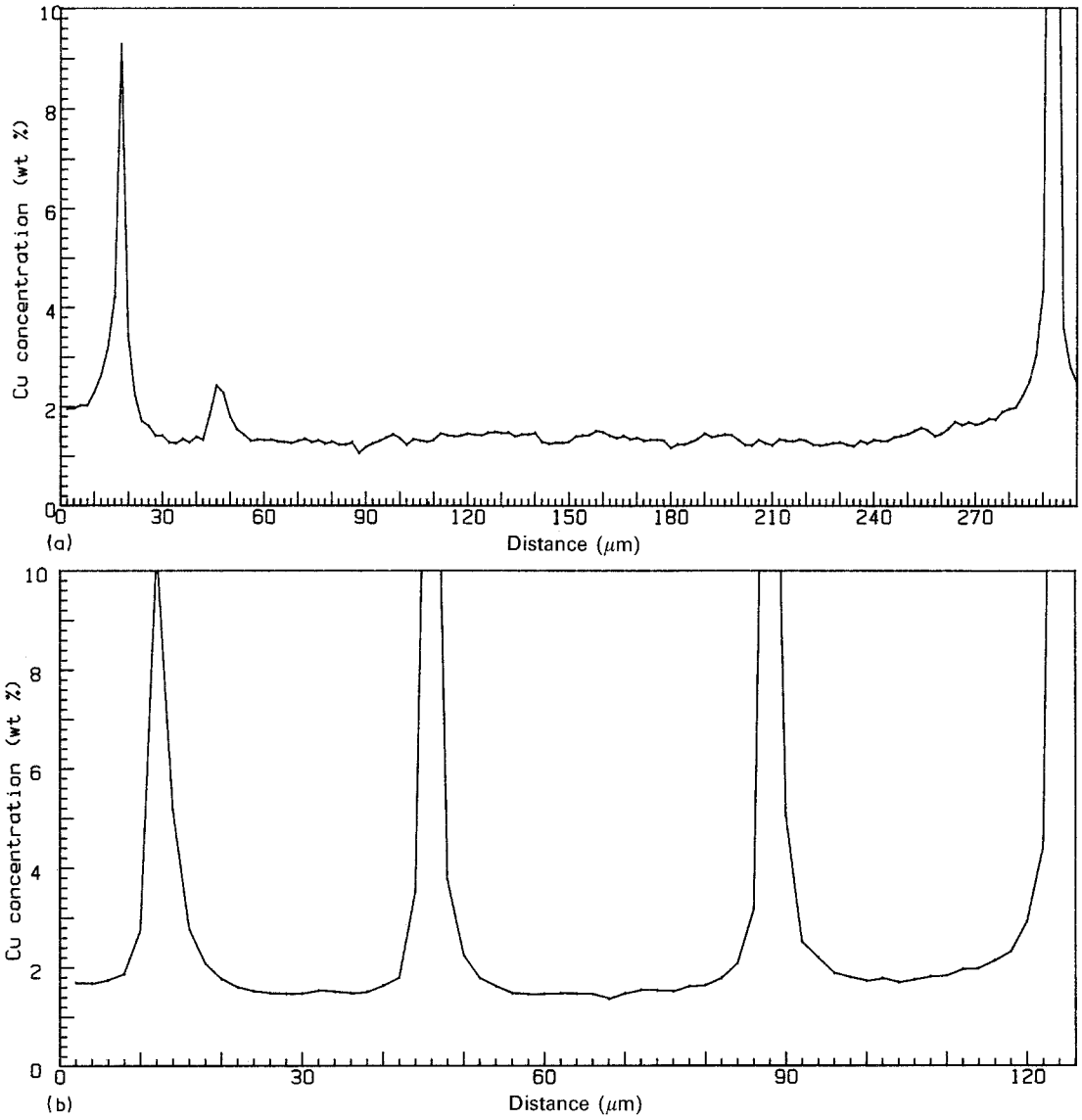

Figure 3 Solute distribution profiles: (a) along the trace shown in Fig. 2a, and (b) along the trace shown in Fig. 2b.

regarded as being equivalent with complete convective mixing. The BF model allows back-diffusion in the solid, while diffusion in the liquid is complete. In the BBF model the back-diffusion in the solid is neglected and diffusion in the liquid is limited. The extent of diffusion in the liquid is quantified by the dendrite tip undercooling constant a (Appendix A, Section A.2). Here, the BBF model is used in a modified interpretation of the original model; in the modified version the effect of a convective mass-flow is included. It appears that the effective equipartition constant k_c is equal to k_0 when convection is absent, while with increasing convective mass-flow its value increases, the maximum being unity in the model (see Equation A19).

Although it has been shown [18] that the microsegregation in dendritic structures is strongly influenced by secondary dendrite arm coarsening, these models take no account of this effect. However, the models are used here for the following reasons: (i) the influence of arm coarsening is relatively weak, when the growth of solid is cellular instead of dendritic, and it was concluded previously [10] that the growth of solid in a stirred bulk liquid is cellular; and (ii) the BBF model has not been applied before to experiments in which the effect of the dendrite tip undercooling parameter a is not small. However, as it is unlikely that the boundary conditions are fulfilled at low solidification rates, we will compare calculated results only with experimental results obtained from quickly cooled samples. Experimental results from slowly cooled samples will be compared with the Scheil distribution, only for reference.

4.1. Calculations

Details of the numerical method of solution of the back-diffusion equation are given in Appendix B. In a comparison of experimental and calculated solute distributions a practical difficulty is that the liquid composition C_0 is unknown at the moment when the mushy zone passes, because the total fraction of solid in the sample (on which C_0 depends) is unknown at that moment. Therefore, calculated concentrations cannot be compared directly with experimental concentrations. However, the following ratio is independent of C_0:

$$F(\xi) = \frac{C_s(\xi) - C_s(0)}{C_s(0)} \quad (1)$$

where ξ is the non-dimensional radial distance to the

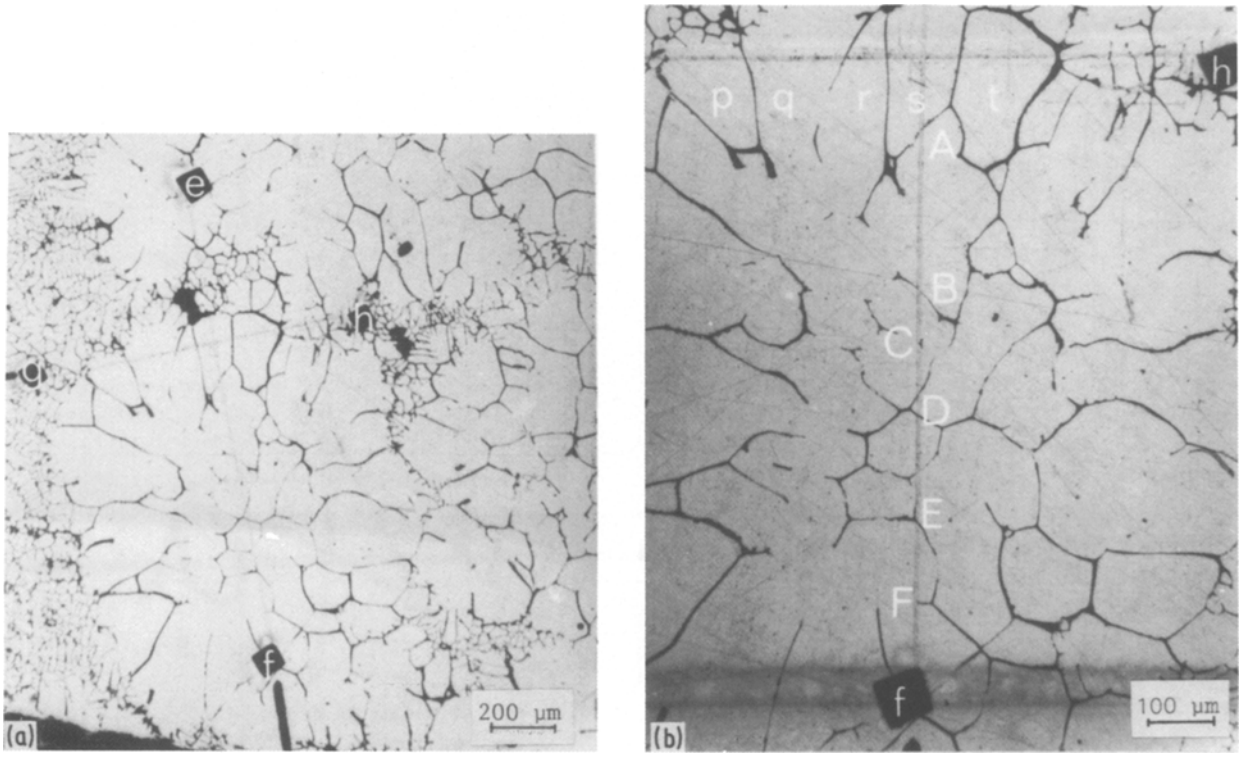

Figure 4 (a) Microstructure of a slowly cooled stir-cast specimen of Al–6Cu (solidification time 228 sec), showing two traces of Cu$K\alpha$ intensity measurement, marked e–f and g–h. (b) Enlarged section of Fig. 4a. Cell boundaries crossed in trace e–f are marked A to F. Cells passed in trace g–h are marked p to t.

axis of the dendritic or cellular arm, $C_s(\xi)$ is the concentration in the solid at the location ξ, and $C_s(0)$ is the concentration at the centre of the dendrite or cellular arm ($\xi = 0$). The ratio $F(\xi)$ was used to analyse experimental solute distribution profiles. General predictions by the Scheil equation, the BF model and the BBF model are presented in Appendix B. In the following, examples of segments of solute distribution profiles obtained from quickly and slowly cooled, stirred and unstirred samples will be discussed.

4.2. Slowly cooled samples

The solute distribution profiles obtained from slowly cooled stir-cast samples are always typically uniform,

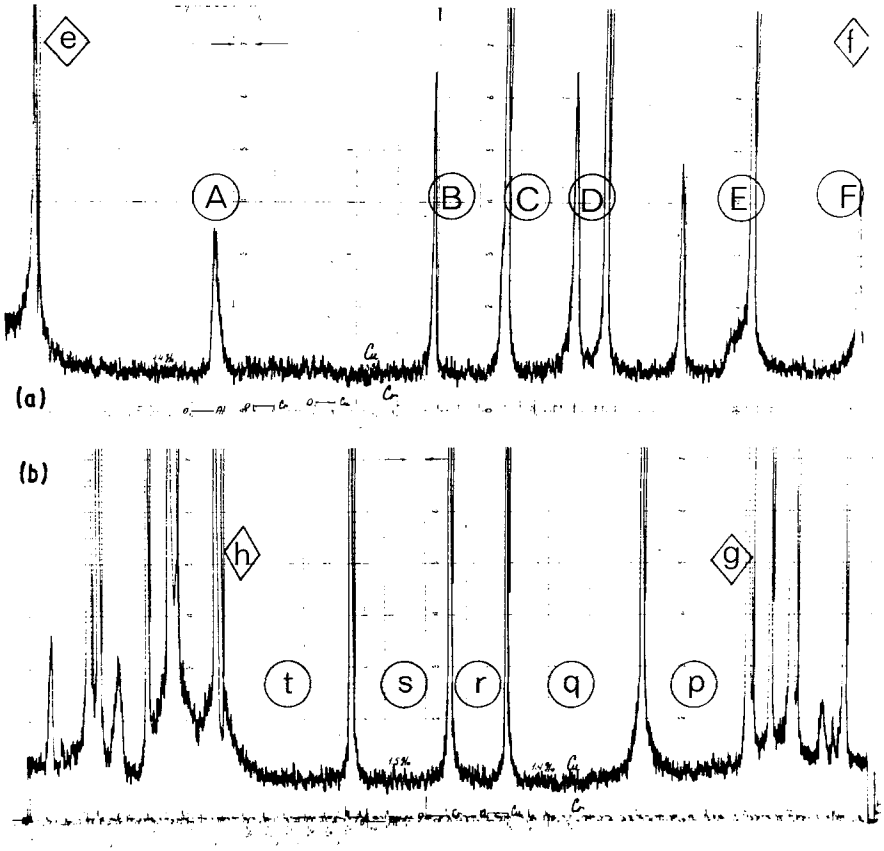

Figure 5 Solute distribution profiles: (a) along trace e–f in Fig. 4a, and (b) along trace g–h in Fig. 4a. Marks correspond to marks in Fig. 4b.

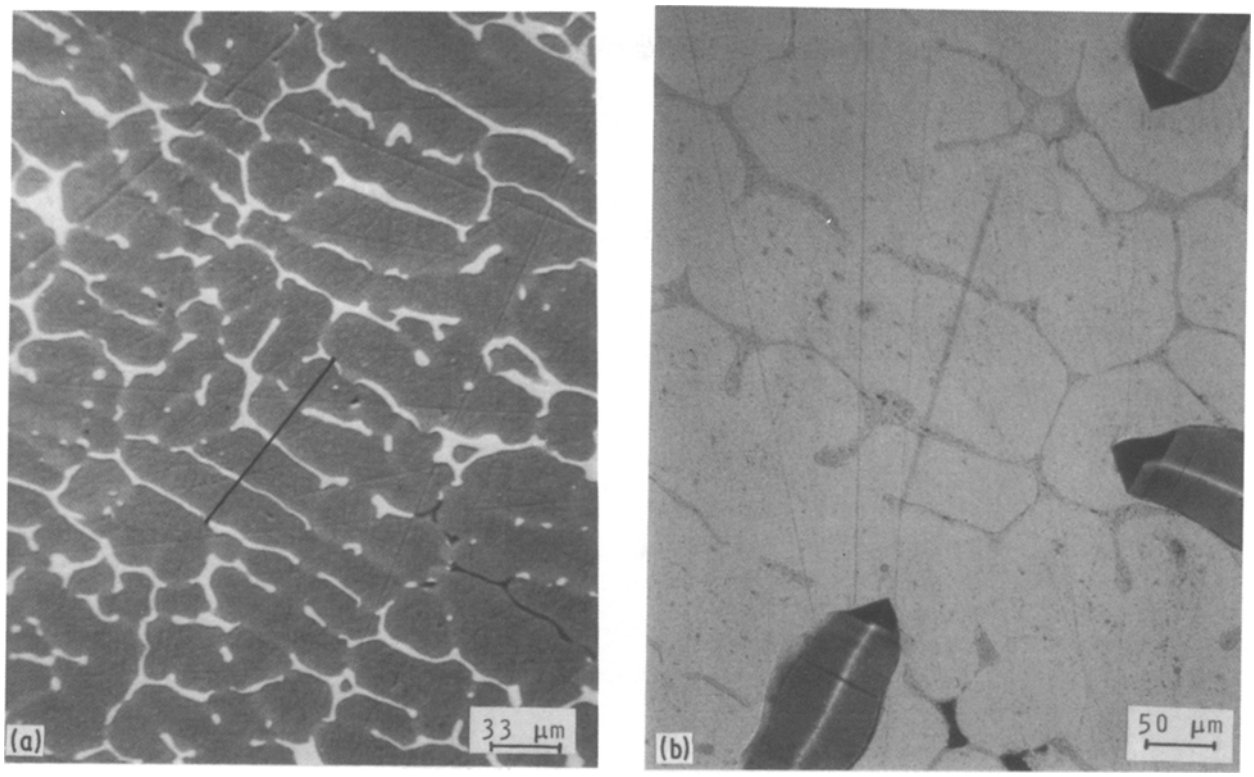

Figure 6 Microstructure of unstirred samples of Al-6Cu, showing traces in transverse direction of Cu$K\alpha$ intensity measurement: (a) quickly cooled specimen (solidification time 8 sec), (b) slowly cooled specimen (solidification time 380 sec).

as illustrated in Fig. 5. Fig. 8a is an example of a graph of $F(\xi)$, showing an experimental result compared to the Scheil distribution. The comparison clearly demonstrates the uniformity of the experimental profile. Only within a distance of $\xi = 0.2$ (about 8 μm) from the phase boundary is the solute concentration significantly different from the average minimum solute concentration. Possibly, the solid within this shell of 8 μm was formed during quenching. This can be deduced from the fact that in many places a dendritic "beard" on primary particle surfaces can be observed, often between 20 and 30 μm wide, which has obviously grown during quenching. As mentioned in Section 3.1.2, the typical uniformity of the profiles obtained from stir-cast samples indicates that solid and liquid were practically in equilibrium before quenching (at about 50% solidified).

The profiles obtained from the naturally cooled unstirred sample are typically different from the ones obtained from slowly cooled stir-cast samples. In Fig. 8b, a segment of a solute distribution profile is compared to the Scheil distribution. This figure shows experimental concentrations that are higher than the ones predicted by the Scheil equation. At first glance this is an unexpected result, since solid back-diffusion should lead to a more uniform distribution. An explanation can be given, based on the fact that the sample was not quenched, but solidified completely during natural cooling. According to Subramanian *et al.* [19], large solute gradients in the solid develop due to the accumulation of solute in the remaining liquid in the final stage of the solidification, and the resulting fall of the rate of solidification. The reason that solute gradients as observed in Fig. 8b were not found in slowly cooled stir-cast samples is that the samples were quenched before such accumulation could occur.

4.3. Quickly cooled samples

In Fig. 9, examples of segments of solute distribution profiles obtained from quickly cooled stirred and unstirred samples are compared to calculated profiles $F(\xi)$ obtained by use of the BF model and the modified BBF model. A general description of the results is given here, before discussing detailed aspects in Sections 4.3.1 and 4.3.2.

Fig. 9a shows graphs of $F(\xi)$ and a segment of a solute distribution profile obtained from a stirred sample. Note that a segment constitutes two sides, one on either side of the central axis of a rosette arm, and that the segment in Fig. 9a is practically symmetric. Fig. 9b shows similar graphs of $F(\xi)$ and a segment of a segregation profile obtained from an unstirred sample. In this example of a secondary dendrite arm, the solute distribution is asymmetric: on one side of the central axis, the profile corresponds well to the Scheil distribution, the other being more uniform. In general, the segments from both stirred and unstirred samples are asymmetric.

As to the shape of the experimental profiles, those from stirred and unstirred samples in Figs 9a and b do not seem to be greatly different. Note, however, that the arm spacing for Fig. 9a is 40 μm, while that for Fig. 9b is 20 μm. Generally, the curves generated from the (modified) BBF model are more compatible with experimental profiles than the curves obtained with the BF model. In particular, the BBF model allows a better description near a phase boundary.

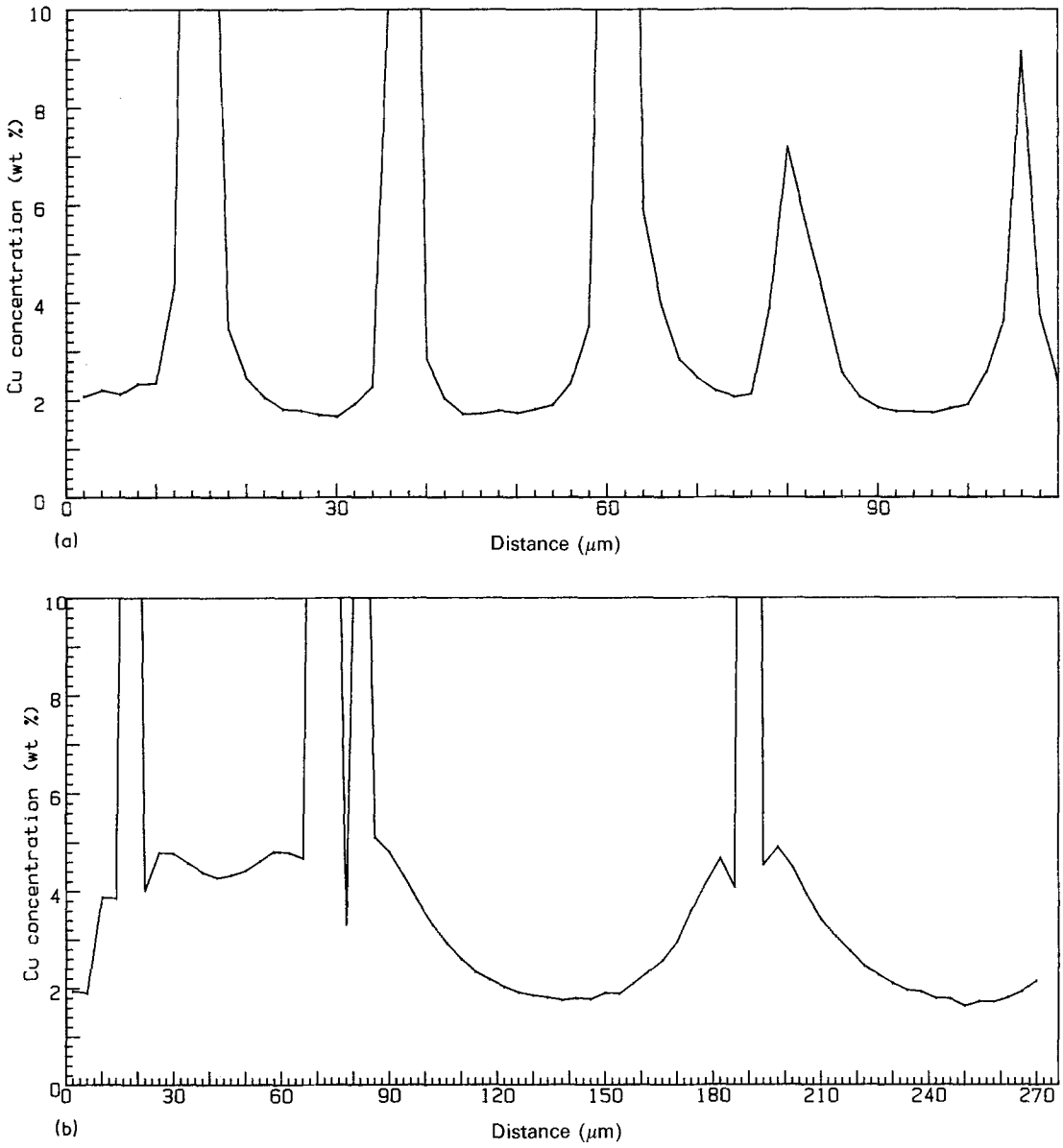

Figure 7 Solute distribution profiles obtained in unstirred Al–6Cu: (a) along the trace shown in Fig. 6a, (b) along the trace shown in Fig. 6b.

4.3.1. Comparison with predictions by the BF model

In the BF model the shape of the solute distribution curve is determined only by the back-diffusion parameter α. The value of α in Equation A3 can be estimated, using the local dendrite arm or cellular arm spacing observed in the microstructure, and the local solidification time. In Table II these values are denoted as α_M. For stirred samples, the local solidification time was taken equal to the total solidification time [8]. For unstirred samples, the local solidification time was obtained from the relation given by Bower *et al.* [11] between local solidification time and secondary dendrite arm spacing (DAS). In Table II the average values of α_M are about 0.05 and 0.1 for the stirred and unstirred samples, respectively.

A number of difficulties arise when the experimental results are compared to predictions by the BF model. Using α as a fitting parameter, the $F(\xi)$ curves obtained from the BF model were hard to fit to the full experi-

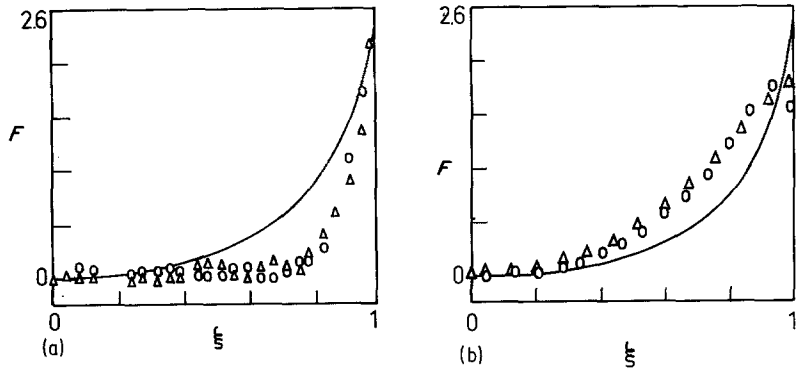

Figure 8 Comparison of experimental solute distributions in slowly cooled Al–6Cu with the Scheil distribution. Solute concentrations on the two sides of the central axis of (○) cellular arm, (△) dendrite arm; (——) Scheil distribution. (a) Stirred specimen (solidification time 228 sec), (b) unstirred specimen (solidification time 380 sec).

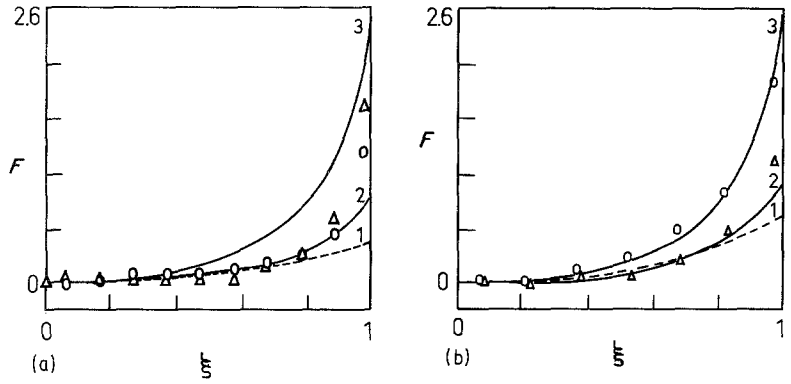

Figure 9 Comparison of observed and calculated solute distributions for quickly cooled Al–6Cu. Observed solute concentrations on the two sides of the central axis of (○) cellular arm, (△) dendrite arm. (a) Stir-cast specimen (solidification time 8 sec). Curves marked 1 to 3 were obtained with the following parameters: (1) $\alpha_c = 1$ (BF model), (2) $\alpha_M = 0.03$, $a = -1.2$ (BBF model), (3) $\alpha = a = 0$ (Scheil distribution). (b) Unstirred specimen (solidification time 8 sec). Curves (1) $\alpha_c = 0.5$ (BF model), (2) $\alpha_M = 0.05$, $a = -0.9$ (BBF model), (3) $\alpha = a = 0$ (Scheil distribution).

mental profiles (see Fig. 9a). In such cases the value was taken corresponding to the best fit to the interior points of the segment. In Table II, the values of α obtained by curve-fitting are denoted as α_c. Note that values of α_c are much greater than those of α_M. In Fig. 10 the minimum solute concentrations $C_s(0)$ are plotted for different values of C_0, as a function of α_c. It is seen that the observed solute minima do not follow these predictions. In addition, it is noted that a comparison of experimental results with predictions by the BF model is troubled by the asymmetry of many segments. For an asymmetric segment, two different values of α_c are obtained corresponding to the same minimum solute concentration $C_s(0)$. The BF model is in conflict with this observation.

It is concluded that the BF model presents difficulties in describing the experimental results. Presumably the assumption of complete diffusion in the liquid is not fullfilled at short solidification times. The importance of limited diffusion in the liquid and limited convective mass-flow will become obvious in the next section.

4.3.2. Comparison with predictions by the modified BBF model

In the modified BBF model the interface solute concentration C_s^i is determined by the two variables a and k_c.

TABLE II Values of α and a obtained for quickly cooled stir-cast and unstirred samples

	Minimum copper concentration, $C_s(0)$ (wt %)	BF model		BBF model	
		α_M	α_c	$-a$	k_c
Stir-cast	1.93	0.04	0.4	0.93	0.165 (2×)
	1.51	0.04	0.5	0.51	0.165
	1.51	0.04	5	0.51	0.58
	1.45	0.05	1	0.45	0.50 (2×)
	1.47	0.04	0.1	0.47	0.165
	1.47	0.04	2	0.47	0.50
	1.41	0.03	1	0.41	0.165 (2×)
	1.75	0.05	0.4	0.75	0.165
	1.75	0.05	0.8	0.75	0.33
Averages	1.6	0.04	1.1	0.6	0.28
Unstirred	1.53	0.05	0.01	0.53	*
	1.53	0.05	0.5	0.53	0.25
	1.78	0.12	0.2	0.78	0.165
	1.78	0.12	1.5	0.78	0.40
	1.76	0.10	0.5	0.76	0.165
	1.76	0.10	1.5	0.76	0.40
	1.76	0.07	0.01	0.76	*
	1.76	0.07	0.5	0.76	0.165
	1.52	0.08	0.01	0.52	* (2×)
	1.83	0.08	0.01	0.83	*
	1.83	0.08	0.5	0.83	0.165
	1.53	0.04	0.2	0.53	0.165 (2×)
	2.29	0.04	0.01	1.3	*
	2.29	0.04	0.1	1.3	0.165
	1.62	0.13	0.5	0.62	0.25 (2×)
	1.59	0.13	0.3	0.59	0.165 (2×)
	2.27	0.22	1	1.3	0.165 (2×)
	1.52	0.10	0.01	0.52	*
	1.52	0.10	0.3	0.52	0.165
	1.44	0.10	0.01	0.44	*
	1.44	0.10	2	0.44	0.67
	1.67	0.10	0.01	0.67	* (2×)
Averages	1.7	0.10	0.4	0.7	0.23

*The experimental points fit the Scheil distribution.

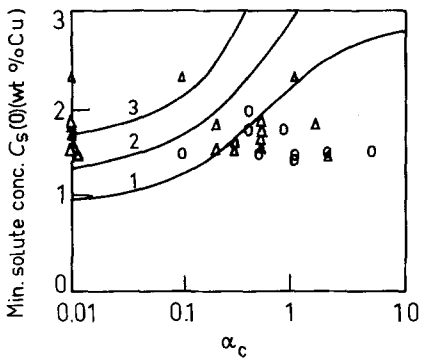

Figure 10 Minimum solute concentration as a function of α_c. Curves represent minimum solute concentrations predicted by the BF model. Observed minima in (○) stirred and (△) unstirred specimens.

Values of a were determined based on work by Doherty *et al.* [16, 17]. They found that the initial dendrite composition depends on the initial growth temperature which is dependent on the heat extraction rate. The initial dendrite composition is given (see Section A.2) by $C_s^i = k_0 C_t = k_0 C_0(1 - a)$, where C_t is the solute content of the liquid at the dendrite tip. Taking C_0 equal to the original liquid composition (6 wt %), and a finding that diffusion in the solid is negligible, it follows that a can be determined from the minimum solute concentration in the centre of the segments. The parameter k_c was determined by curve-fitting. The values of a and k_c thus obtained are listed in Table II.

It can be verified in Table II that average values of a are about equal for stirred and unstirred samples, in agreement with the fact that the experiments were carried out under the same thermal conditions, which should lead to similar initial growth temperatures. It is found that solute minima in adjacent dendrite or cellular arms may be different. Also, the spacings of individual dendrite arms or cellular arms show local differences, which involve locally different curvature undercoolings. From these observations it is concluded that the dendrite tip undercooling can be locally different. This means that adjacent arms do not grow at the same rate.

As to the values of k_c, it is seen in Table II that in most cases of stirred and unstirred samples, a fit of the solute distribution profiles to $F(\xi)$ curves produced by the (modified) BBF model can be obtained for a value of k_c equal to or greater than k_0. Thus, in the modified BBF model it follows naturally that asymmetry of solute distribution profiles is due to locally different flow intensities, even in unstirred samples; interdendritic fluid flows develop as a result of contraction strains, solid–liquid contraction and capillary action. Fluid flow intensities may vary from one place to another, giving different values of k_c and influencing the interface concentrations.

About a third of the profiles of the unstirred samples (indicated with asterisks in Table II) are found to correspond to the Scheil distribution. These cases are not described by the BBF model or the modified model, since these predict a more uniform distribution in the case where α is non-zero. To explain this result, we must assume that convective transport of solute cancels the accumulation of solute in the liquid, represented by a. Then, there is no net transport of solute, a condition equivalent to that of complete diffusion in the liquid, described by the Scheil equation.

5. Discussion and conclusions

The analysis in the previous sections shows that the modified BBF model allows a reasonable description of the microsegregation in both stirred and unstirred quickly cooled samples. Based on the modified BBF equation (Equation A19) and the value of a and k_c in Table II, it can be concluded that the solute in intercellular liquid is transported both by diffusion and convection. The mass-flow by diffusion is represented by the parameter a, and the convective mass-flow by the parameter k_c. Considering the average values of k_c for the stirred and unstirred samples, 0.28 and 0.23 respectively, it follows that the mean values of V/R in Equation A20 are 0.11 and 0.06 for stirred and unstirred samples, respectively. This shows that the intercellular convective mass-flow is increased by stirring in the melt.

An idea of the ratio of the mass-flows by convection and diffusion (equivalent to the non-dimensional Peclet number) is obtained simply from the quotient of $k_c - k_0$ and a: for the stir-cast samples, $Pe = (k_c - k_0)/a$ is about 0.2, and for the unstirred samples about 0.1. These values, both being smaller than unity, indicate that diffusion in the liquid is predominant. Obviously, at high cooling rates (i.e. when $-a$ is large), the influence of stirring during the solidification of a semi-solid slurrry is fairly limited.

It is now clear why the BF model fails to give a good description. Firstly, a considerable dendrite tip or cell tip undercooling develops due to a high cooling rate in the liquidus region. As a consequence the diffusion in the solid is negligible compared to that in the liquid. Secondly, the microsegregation was influenced by convection, also in the unstirred samples. This follows from the observed asymmetry of solute distributions and from the fact that k_c is often greater than k_0.

Acknowledgement

The authors are grateful to Professor B. M. Korevaar for helpful discussions and critical reading of the manuscript.

Appendix A: Solute redistribution equations

A.1. The Brody–Flemings model

For a plate-like dendritic solidification geometry, Brody and Flemings [13] derived the following equation which describes the interface solute concentration C_s^i as a function of the local fraction solid f_s, in the case where the growth velocity decreases parabolically with increasing time:

$$C_s^i = k_0 C_0 \{1 - f_s[1 - 2\Omega(\alpha)k_0]\}^{(k_0 - 1)/[1 - 2\Omega(\alpha)k_0]} \quad \text{(A1)}$$

where C_0 is the solute content of the liquid just before the mushy zone passes, k_0 is the equilibrium partition ratio, and $\Omega(\alpha)$ is defined by [14]

$$\Omega(\alpha) = \alpha\left[1 - \exp\left(-\frac{1}{\alpha}\right)\right] - \tfrac{1}{2}\exp\left(-\frac{1}{2\alpha}\right) \quad \text{(A2)}$$

The constant α is related to the dendritic arm spacing λ, taken as twice the diffusion path length L, by the equation

$$\alpha = \frac{D_s t_s}{L^2} = \frac{4D_s t_s}{\lambda^2} \quad \text{(A3)}$$

In this equation D_s is the diffusion coefficient of the solute in the solid phase and t_s is the local freezing time. In the original treatment, the local fraction of solid is defined by [13]

$$f_s = r^i/L \quad \text{(A4)}$$

where r^i denotes the position of the interface with respect to the dendrite axis. For a cylindrical arm we have

$$f_s = \pi\left(\frac{r^i}{2L}\right)^2 \quad \text{(A5)}$$

Equation A2 shows that as α approaches zero, $\Omega(\alpha) \rightarrow 0$ and Equation A1 reduces to the Scheil equation, while if α goes to infinity, $\Omega(\alpha) \rightarrow 0.5$ and Equation A1 reduces to the equilibrium lever rule. Equation A1 is known as the Brody–Flemings model. It was derived under the assumption of complete diffusion in the liquid.

A.2. The Bower–Brody–Flemings model

In Fig. A1, a schematic representation is given of the cellular type of solidification. It is assumed that the solidification is unidirectional and started at a chilled mould surface. Bower *et al.* [11, 20] make the following assumptions:

(i) the partition ratio k_0, liquidus slope m_L ($m_L < 0$), dendrite tip velocity R, thermal gradient G_L, liquid diffusion coefficient D_L, and liquid density are constant;

(ii) diffusion in the solid is negligible;

(iii) solidification is steady-state, i.e. initial transient effects are neglected; and

(iv) constitutional supercooling in the mushy zone is negligible.

The gradient of the equilibrium liquidus temperature G_L^* is defined by

$$G_L^* = m_L \frac{\partial C_L}{\partial x} \quad \text{(A6)}$$

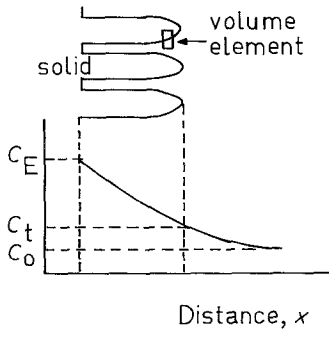

Figure A1 Schematic diagram of cellular dendrites in the solid–liquid region (after [20]), and the steady-state solute distribution in intercellular liquid. C_E represents the eutectic liquidus concentration, C_t the solute concentration in the liquid at the cell tips and C_0 the original solute concentration in the liquid.

where C_L is the solute content in the liquid. By Assumption (iv), the equilibrium liquidus temperature distribution $T_L^*(x)$ in the mushy zone is equal to the actual temperature distribution $T_L(x)$. Therefore, in Equation A6 G_L^* may be substituted by the actual thermal gradient G_L in the system. In the volume-element shown in Fig. A1, the mass balance is written as

$$\frac{\partial}{\partial x}\left(D_L f_L \frac{\partial C_L}{\partial x}\right) = f_L \frac{\partial C_L}{\partial t} + C_L(1 - k_0)\frac{\partial f_L}{\partial t} \quad \text{(A7)}$$

For steady-state solidification

$$\frac{\partial f_L}{\partial x} = -\frac{1}{R}\frac{\partial f_L}{\partial t} \qquad \frac{\partial C_L}{\partial x} = -\frac{1}{R}\frac{\partial C_L}{\partial t} \quad \text{(A8)}$$

The dendrite tip undercooling constant a ($a < 0$) is defined by

$$a = \frac{D_L G_L^*}{m_L C_0 R} \quad \text{(A9)}$$

Substitution of Equations A8 and A9 in Equation A7 yields

$$-\frac{dC_L}{C_L(1 - k_0) + aC_0} = \frac{df_L}{f_L} \quad \text{(A10)}$$

Integrating the left-hand part of this equation from C_t to C_L and the right-hand part from 1 to f_L, the following equation is obtained:

$$f_L = \left(\frac{C_t(1 - k_0) + aC_0}{C_L(1 - k_0) + aC_0}\right)^{1/(1-k_0)} \quad \text{(A11)}$$

where C_t is the solute content in the liquid at the cell tips. In the steady state, the requirement of no solute accumulation at the cell-tips gives

$$C_t = C_0(1 - a) \quad \text{(A12)}$$

Substituting in Equation A11 gives

$$C_s^i = k_0 C_0\left[\frac{a}{k_0 - 1} + \left(1 - \frac{ak_0}{k_0 - 1}\right)(1 - f_s)^{(k_0 - 1)}\right] \quad \text{(A13)}$$

Writing Equation A12 in terms of temperature depression of the dendrite tip, it is found that

$$\Delta T_t = T_L - T_t = am_L C_0 \quad \text{(A14)}$$

where T_L is the liquidus temperature of the alloy and T_t the dendrite tip temperature.

A.3. The modified Bower–Brody–Flemings model

Consider a rosette-type particle floating in a stirred liquid and growing in the radial direction. In addition to the assumptions made by Bower *et al.* [11], we assume that the temperature in the suspended particle is constant. There is then a negative thermal gradient and a positive solute gradient at the cell-tips; therefore

$$T_L^*(x) \neq T_L(x) \quad \text{(A15)}$$

and G_L^* in Equation A6 may not be substituted by the actual thermal gradient in the system. Taking account of a convective mass-flow in the mushy zone, we may write the following mass-balance in the volume element

in Fig. A1:

$$\frac{\partial}{\partial x}\left(D_L f_L \frac{\partial C_L}{\partial x}\right) - \frac{\partial}{\partial x}(V f_L C_L) = f_L \frac{\partial C_L}{\partial t} + C_L(1 - k_0)\frac{\partial f_L}{\partial t} \quad \text{(A16)}$$

where V represents the velocity of the convective mass-flow. It is assumed that V is constant in the intercellular liquid away from the cell tips, and decreases rapidly to zero nearby the tips. Substituting Equations A8 and A9 in Equation A16, we obtain

$$-\frac{dC_L}{C_L[1 - k_0 - (V/R)] + aC_0} = \frac{df_L}{f_L} \quad \text{(A17)}$$

and after integration similar to Equation A10

$$f_L = \left(\frac{C_t[1 - k_0 - (V/R)] + aC_0}{C_L[1 - k_0 - (V/R)] + aC_0}\right)^{[1-(V/R)]/[1-k_0-(V/R)]} \quad \text{(A18)}$$

As $V = 0$ at the cell tips, Equation A12 is equally valid here, and substitution in Equation A18 gives

$$C_s^i = k_0 C_0\left[\frac{a}{k_c - 1} + \left(1 - \frac{ak_c}{k_c - 1}\right) \times (1 - f_s)^{(k_c-1)/[1-(V/R)]}\right] \quad \text{(A19)}$$

where

$$k_c = k_0 + \frac{V}{R} \quad \text{(A20)}$$

Equation A19 is the modified BBF-equation in which the effect of a convective mass-flow in the intercellular liquid is taken into account. Based on this equation it is concluded that the microsegregation is influenced by convection if V/R is not negligible with respect to k_0. The effect of V/R is to reduce the solute gradient in the direction parallel to the axes of the cells. The parameter a can take values between zero and the minimum: $a_m = (k_c - 1)/k_c$. If $a = a_m$, the solute distribution is uniform with $C_s^i = (k_0/k_c)C_0 =$ constant. The maximum convective mass-flow is given by $V/R = 1 - k_0$, when all rejected solute is transported, so that no solute gradient in the intercellular liquid exists. The liquid composition is then constant and equal to C_0. There is no solute enrichment at the interface ($k_c = 1$, $a = 0$); the cell-tip undercooling is zero, and the solid composition formed is equal to $k_0 C_0$.

Appendix B: Calculations and general predictions

B.1. Microsegregation model

For the cylindrical geometry of Fig. B1, the boundary problem constitutes the diffusion equation describing the solute concentration in the solid, C_s:

$$\frac{\partial C_s}{\partial t} = D_s\left(\frac{1}{r}\frac{\partial C_s}{\partial r} + \frac{\partial^2 C_s}{\partial r^2}\right) \quad \text{(B1)}$$

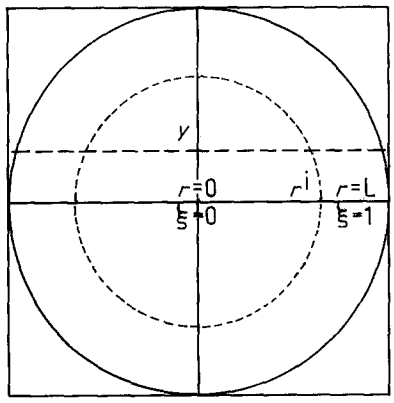

Figure B1 Schematic diagram of the cylindrical cell morphology.

with the boundary conditions

$$t \geqslant 0,\ r = r^i;\ r^i = \frac{L}{t_s^{1/2}} t^{1/2} \quad \text{(B2)}$$

$$t \geqslant 0,\ r = r^i;\ C_s^i \quad \text{(B3)}$$

as defined by Equation A1 or A19

$$t \geqslant 0,\ r = 0;\ \partial C_s/\partial r = 0 \quad \text{(B4)}$$

$$t \geqslant 0,\ r = r^i;\ f_s = \pi(r^i/2L)^2 \quad \text{(B5)}$$

Equation B2 is used in accordance with the work by Brody and Flemings [13], and by Clyne and Kurz [14]. Upon introduction of the following non-dimensional quantities

$$\Gamma(\xi) = \frac{C_s(\xi) - k_0 C_0}{k_0 C_0} \qquad \varrho = \frac{r^i}{L}$$

$$\xi = \frac{r}{L} \qquad \tau = \frac{D_s t}{L^2} \quad \text{(B6)}$$

the diffusion equation B1 is rewritten as

$$\frac{\partial \Gamma}{\partial \tau} = \frac{1}{\xi}\frac{\partial \Gamma}{\partial \xi} + \frac{\partial^2 \Gamma}{\partial \xi^2} \quad \text{(B7)}$$

and the boundary conditions as

$$\tau \geqslant 0,\ \xi = \varrho;\ \varrho = (\tau/\alpha)^{1/2} \quad \text{(B8)}$$

$$\tau \geqslant 0,\ \xi = \varrho;\ \Gamma^i = C_s^i/(k_0 C_0 - 1) \quad \text{(B9)}$$

$$\tau \geqslant 0,\ \xi = 0;\ \partial\Gamma/\partial\xi = 0 \quad \text{(B10)}$$

$$\tau \geqslant 0,\ \xi = \varrho;\ f_s = \pi\varrho^2/4 \quad \text{(B11)}$$

The spatial discretization of Equation B7 is achieved by dividing the interval of L into n interval of length $\Delta\xi$. Then ξ is equal to $i\Delta\xi$, where i runs from 0 to n. The time discretization involves a series of discrete time periods τ^k, where k denotes the time step. The τ^k values correspond with the solutions Γ^k for the interface positions ϱ^k. The interval $\Delta\tau^k$ is the time required for the solid–liquid interface to advance exactly one interval $\Delta\xi$ in the kth time step. Replacing the spatial derivatives by central difference quotients, and the time derivative by a backward difference quotient,

$$\frac{\partial \Gamma}{\partial \xi} = \frac{\Gamma_{i+1}^k - \Gamma_{i-1}^k}{2\Delta\xi} \quad \text{(B12)}$$

$$\frac{\partial^2\Gamma}{\partial\xi^2} = \frac{\Gamma_{i-1}^k - 2\Gamma_i^k + \Gamma_{i+1}^k}{(\Delta\xi)^2} \quad \text{(B13)}$$

$$\frac{\partial\Gamma}{\partial\tau} = \frac{\Gamma_i^k - \Gamma_i^{k-1}}{\Delta\tau^k} \quad \text{(B14)}$$

the following difference scheme is obtained for Equation B7:

$$-\left(1 - \frac{1}{2i}\right)\Gamma_{i-1}^k + \left(2 + \frac{1}{P^k}\right)\Gamma_i^k - \left(1 + \frac{1}{2i}\right)\Gamma_{i+1}^k = \frac{\Gamma_i^{k-1}}{P^k} \quad \text{(B15)}$$

where $P^k = \Delta\tau^k/(\Delta\xi)^2$. The value of P^k is obtained directly from the boundary condition of Equation B8:

$$P^k = 2\alpha\varrho^k/\Delta\xi \quad \text{(B16)}$$

The following ratio is independent of C_0:

$$F = \frac{C_s(\xi) - C_s(0)}{C_s(0)} = \frac{\Gamma(\xi) - \Gamma(0)}{\Gamma(0) + 1} \quad \text{(B17)}$$

and can be evaluated directly from experimental concentration profiles. The ratio was calculated for different values of α, a and k_c, and in different planes of observation defined by the parameter y in Fig. B1. The latter was varied to check errors introduced in case the actual plane of observation is not a normal plane (i.e. when $y \neq 0$). In general y will be greater than zero, and the observed profile will be more uniform than the actual solute distribution. Also, the observed spacing ϱ will be smaller than the real spacing. It was found that the influence of a shift of the plane of observation on the calculated curve is small if y is smaller than 0.2. The same was found for other values of α, also when a was non-zero. Because the profiles were taken in cellular arms and dendrite arms with a larger than average spacing, we expect that for most of the measurements y is smaller than 0.2. Therefore, the influence of deviations from the normal plane was neglected.

In this work an average value is used for D_s: $10^{-12}\,m^2\,sec^{-1}$, corresponding to a temperature of 900 K [21]. The value used for the equipartition ratio k_0 was 0.165.

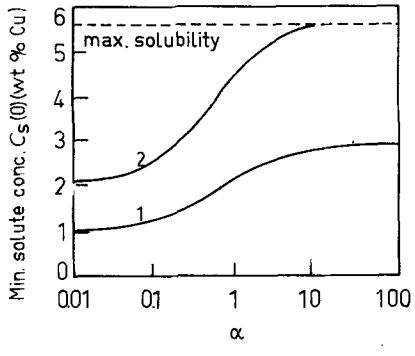

Figure B2 Minimum solute concentration at the axis of a dendrite arm, $C_s(0)$, as a function of α, for different values of C_0, predicted by the BF model. Curves: (1) C_0 = 6 wt % Cu, (2) C_0 = 12 wt % Cu.

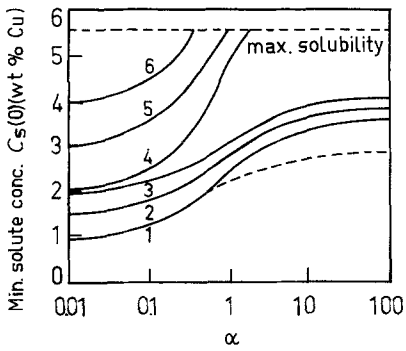

Figure B3 Minimum solute concentration at the axis of a dendrite arm, $C_s(0)$, as a function of α, for different values of C_0, and a, predicted by the BBF model. Curves: (1 to 3) C_0 = 6 wt % Cu and a = 0, −0.5 and −1, respectively; (4 to 6) C_0 = 12 wt % Cu and a = 0, −0.5 and −1, respectively. The dashed curve corresponds to the result predicted by the BF model for C_0 = 6 wt % Cu (Curve 1 in Fig. B2).

B.2. General predictions

In this section, the general results predicted by the Scheil equation, the BF model and the modified BBF model are presented. In Fig. B2, the minimum concentration $C_s(0)$ predicted by the BF equation is plotted as a function of α, for different values of C_0. When α approaches infinity, the lower curve approaches a limit which is equal to the interface concentration for the maximum solid fraction attainable in the geometry of Fig. B1. For sufficiently large solute contents this limit is the maximum solid solubility. It can be seen for C_0 = 6 wt % that the minimum copper concentration $C_s(0)$ increases from 1 wt % (i.e. the value of $k_0 C_0$) for small values of α to about 1.25 wt % when α = 0.1. In general, diffusion in the solid contributes little to the increase in minimum solute concentration, if $\alpha < 0.1$. Of course, C_0 increases during the solidification of a sample, so higher minima are possible in locations where C_0 was greater. Using the modified BBF equation A19, similar plots can be obtained for different values of a and k_c. Fig. B3 is an example for $k_c = k_0$, and different values of a. It is seen that the minimum solute concentrations increase with decreasing values of a. From Equation A12 it is clear that this is a consequence of a higher cell tip concentration. The curve for a = 0 is identical to the result obtained with the Scheil

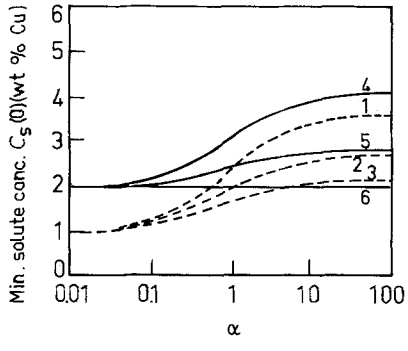

Figure B4 Minimum solute concentration at the axis of a dendrite arm, $C_s(0)$, as a function of α, for C_0 = 6 wt % Cu and different values of a and k_c, predicted by the BBF model. Curves: (1 to 3) a = 0 and $k_c = k_0$, $2k_0$ and $3k_0$, respectively; (4 to 6) a = −1 and $k_c = k_0$, $2k_0$ and $3k_0$, respectively.

equation, and is compared to the prediction by the BF equation (dashed line). The difference is due to different predicted interface concentrations.

Note that in fact none of the models predict the correct interface solute concentration C_s^i, since the assumptions merely allow an approximate description of the real solidification conditions. The comparison in Fig. B3 shows, here for $C_0 = 6$ wt % Cu, that errors can be expected to remain small provided α is not greater than unity. The following observations can be made in Fig. B3: (i) the interface solute concentrations C_s^i predicted by the Scheil equation and the BF model are similar if α is smaller than unity, and (ii) in the case where a is a non-zero the influence of back-diffusion in the solid is negligible, if $a < 0.1$. Under these conditions, the modified BBF model can be used as a single equation to predict experimental solute distribution profiles.

Fig. B4 demonstrates the influence of convective solute transport, through increasing values of k_c. It can be seen in Fig. B4 that the minimum solute concentration decreases with increasing k_c, due to solute transport in the liquid away from the interface. For small α (short solidification time) the effect is smaller than for large α.

References

1. M. C. FLEMINGS, R. G. RIEK and K. P. YOUNG, *Mater. Sci. Eng.* **25** (1976) 103.
2. *Idem, AFS Int. Cast Met. J.* **1** (1976) 11.
3. M. C. FLEMINGS *et al.*, in "Rheocasting", Proceedings of Workshop, Metals and Ceramics Information Center, Batelle Columbus Laboratories, Columbus, Ohio, 1978, edited by R. D. French and H. S. Hodi (Metals and Ceramics Information Centre, Columbus, 1978).
4. P. A. JOLY and R. MEHRABIAN, *J. Mater. Sci.* **11** (1976) 1393.
5. A. VOGEL, R. D. DOHERTY and B. CANTOR, in Proceedings of International Conference on Solidification and Casting of Metals, University of Sheffield, July 1977 (Metals Society, London, 1979) p. 518.
6. H. I. LEE, R. D. DOHERTY, E. A. FEEST and J. M. TITCHMARSH, in Proceedings of International Conference on Soldification Technology in the Foundry and Casthouse, Warwick, Coventry, 1980 (The Metals Society, London, 1983) p. 119.
7. R. D. DOHERTY, H. I. LEE and E. A. FEEST, *Mater. Sci. Eng.* **65** (1984) 181.
8. J. M. M. MOLENAAR, F. W. H. C. SALEMANS and L. KATGERMAN, *J. Mater. Sci.* **20** (1985) 4335.
9. J. M. M. MOLENAAR, R. J. SMEULDERS, L. KATGERMAN and W. H. KOOL, *ibid.* **21** (1986) 389.
10. J. M. M. MOLENAAR, R. J. SMEULDERS and W. H. KOOL, *ibid.* **22** (1987) 1102.
11. T. F. BOWER, H. D. BRODY and M. C. FLEMINGS, *Trans. AIME* **236** (1966) 624.
12. M. C. FLEMINGS, "Solidification Processing" (McGraw-Hill, New York, 1974) p. 34.
13. H. D. BRODY and M. C. FLEMINGS, *Trans. AIME* **236** (1966) 615.
14. T. W. CLYNE and W. KURZ, *Met. Trans.* **12A** (1981) 965.
15. R. M. SHARP and A. HELLAWELL, *J. Crystal Growth* **11** (1971) 77.
16. R. D. DOHERTY, E. A. FEEST and K. HOLM, *Met. Trans.* **4** (1973) 115.
17. E. A. FEEST and R. D. DOHERTY, *ibid.* **4** (1973) 125.
18. M. C. FLEMINGS, "The solidification of Metals", ISI Publication No. 110 (Iron and Steel Institute, London, 1967) p. 277.
19. S. V. SUBRAMANIAN, C. W. HAWORTH and D. H. KIRKWOOD, *J. Iron Steel Inst.* **206** (1968) 1124.
20. M. C. FLEMINGS, "Solidification Processing" (McGraw-Hill, New York, 1974) pp. 77–83.
21. J. B. MURPHY, *Acta Metall.* **9** (1961) 563.

Received 5 October 1987
and accepted 29 January 1988